Nanoscale

Planar B₄₁⁻ and B₄₂⁻ clusters with double-hexagonal vacancies†

Hui Bai, [ID] ‡[a,b] Teng-Teng Chen, [ID] ‡[b] Qiang Chen,‡[c] Xiao-Yun Zhao,[c] Yang-Yang Zhang,[d] Wei-Jia Chen, [ID] [b] Wan-Lu Li, [ID] [d] Ling Fung Cheung, [ID] [b] Bing Bai,[a,b] Joseph Cavanagh,[b] Wei Huang, [ID] [a] Si-Dian Li, [ID] *[c] Jun Li [ID] *[d,e] and Lai-Sheng Wang [ID] *[b]

Since the discovery of the B₄₀ borospherene, research interests have been directed to the structural evolution of even larger boron clusters. An interesting question concerns if the borospherene cages persist in larger boron clusters like the fullerenes. Here we report a photoelectron spectroscopy (PES) and computational study on the structures and bonding of B₄₁⁻ and B₄₂⁻, the largest boron clusters characterized experimentally thus far. The PE spectra of both clusters display broad and complicated features, suggesting the existence of multiple low-lying isomers. Global minimum searches for B₄₁⁻ reveal three low-lying isomers (**I–III**), which are all related to the planar B₄₀⁻ structure. Isomer **II** (C_s, ^{1}A′) possessing a double hexagonal vacancy is found to agree well with the experiment, while isomers **I** (C_s, ^{3}A″) and **III** (C_s, ^{1}A′) both with a single hexagonal vacancy are also present as minor isomers in the experiment. The potential landscape of B₄₂⁻ is found to be much more complicated with numerous low-lying isomers (**VII–XII**). The quasi-planar structure **VIII** (C_1, ^{2}A) containing a double hexagonal vacancy is found to make major contributions to the observed PE spectrum of B₄₂⁻, while the other low-lying isomers may also be present to give rise to a complicated spectral pattern. Chemical bonding analyses show isomer **II** of B₄₁⁻ (C_s, ^{1}A′) and isomer **VIII** of B₄₂⁻ (C_1, ^{2}A) are π aromatic, analogous to that in the polycyclic aromatic hydrocarbon $C_{27}H_{13}^+$ (C_{2v}, ^{1}A₁). Borospherene cage isomers are also found for both B₄₁⁻ and B₄₂⁻ in the global minimum searches, but they are much higher energy isomers.

1. Introduction

Elemental boron exhibits a rich variety of interesting allotropes, consisting of different three-dimensional (3D) polyhedral cages due to the electron deficiency of boron.[1,2] Over the past two decades, the structures and bonding of size-selected boron clusters have been systematically investigated by joint experimental and theoretical techniques up to 40 atoms,[3–11] primarily using photoelectron spectroscopy (PES).[12–39] In contrast to bulk boron and borane compounds,[1,2,40] where 3D polyhedral cages are dominant, size-selected boron clusters have been found mainly to consist of planar or quasi-planar (2D) structures. One of the most interesting boron clusters in this size range is B₄₀⁻, the largest boron cluster that has been experimentally characterized to date.[29] It was found to have a 2D global minimum structure, but with an energetically accessible fullerene-like cage isomer, which was observed experimentally and named borosphere-ne.[27] Remarkably, the neutral B₄₀ borospherene is overwhelmingly more stable than any 2D isomers. It is an extremely stable electronic system with a huge energy gap between its highest occupied molecular orbital (HOMO) and its lowest unoccupied MO (LUMO). The B₃₉⁻ cluster was subsequently found to have two nearly degenerate axially chiral borosphere-ne isomers competing for the global minimum.[31] Seashell-like C_2 B₂₈⁻ and C_s B₂₉⁻ borospherenes have also been observed in PES experiments as minor isomers,[33,34,41] though their global minima are comprised of 2D structures.

All 2D boron clusters consist of a periphery with strong classical two-center two-electron (2c–2e) B–B localized σ bonds

[a]Key Laboratory of Coal Science and Technology of Ministry of Education and Shanxi Province, Taiyuan University of Technology, Taiyuan 030024, Shanxi, China
[b]Department of Chemistry, Brown University, Providence, Rhode Island 02912, USA. E-mail: lai-sheng_wang@brown.edu
[c]Nanocluster Laboratory, Institute of Molecular Science, Shanxi University, Taiyuan 030006, Shanxi, China. E-mail: lisidian@sxu.edu.cn
[d]Department of Chemistry & Key Laboratory of Organic Optoelectronics and Molecular Engineering of Ministry of Education, Tsinghua University, Beijing 100084, China. E-mail: junli@tsinghua.edu.cn
[e]Department of Chemistry, Southern University of Science and Technology, Shenzhen 518055, China
†Electronic supplementary information (ESI) available. See DOI: 10.1039/c9nr09522e
‡These authors contributed equally to this work.

and inner atoms with weaker delocalized σ and π bonding.[5–7,9–39] The main structural features of the interior atoms in the 2D boron clusters are the B_3 triangles, interspersed with different defects, including tetragonal, pentagonal, hexagonal or double hexagonal vacancies (DHV). The weaker delocalized interior bonding and the presence of defects give rise to the fluxionality known in 2D boron clusters.[5–7,20–30,42–45] More interestingly, the delocalized π bonds in 2D boron clusters have been found to be similar to those in the polycyclic aromatic hydrocarbons (PAHs), and the 2D boron clusters have been considered as all-boron analogs of PAHs.[5–7,15,16,19–21] The size of the vacancy in 2D boron clusters increases with the cluster size from tetragonal to pentagonal, hexagonal and DHV.[5,6,9–11] The B_n^- (n = 26, 27, 30–34, 36) clusters were found to contain a single hexagonal vacancy,[26,32,37–39] whereas B_n^- (n = 35, 37, 38, 40) clusters all contain a DHV.[29,30,35] Hexagonal vacancies with different hole densities and arrangements had been predicted computationally to form stable and perfectly planar monolayer borons.[46–52] Therefore, the first discovery of the planar B_{36} cluster with a central hexagonal vacancy provided indirect experimental evidence for the viability of planar 2D borons and led to the coining of the name "borophene" in anticipation of their eventual synthesis as a new class of 2D materials.[26] The subsequent finding of the B_{35}^- cluster with a DHV provided further confirmation of the viability of borophenes.[30] Remarkably, within less than two years, two research teams successfully fabricated borophenes on Ag substrates using atomic vapor deposition methods,[53,54] as first proposed computationally.[55,56] The most stable borophene observed experimentally has the so-called χ^3 form with a hole density of η = 1/5. The χ^3 borophene is composed of rows of adjacent hexagonal vacancies connected by zigzag boron double chains,[54,57,58] similar to the hexagonal vacancies in the B_{35} and B_{36} clusters, which were viewed as building blocks for borophenes.[26,30]

A crucial question concerns the structures of boron clusters beyond B_{40}. Will the borospherene structure persist like in the fullerenes? Or will 2D structures continue to dominate leading up to borophenes? Numerous calculations on larger boron clusters beyond B_{40} have been reported.[59–70] Large boron fullerenes have been suggested,[71–75] though the initially proposed B_{80} fullerene was found to be a much higher energy isomer.[76–79] However, there have been no experimental studies beyond B_{40}. It still remains a question which structural growth pattern will be favored for larger boron clusters. Here we report a PES experimental and quantum chemical study of the B_{41}^- and B_{42}^- clusters. Experimental PE spectra of both B_{41}^- and B_{42}^- have been obtained, both showing fairly complicated photodetachment features and suggesting the possible existence of multiple isomers. Major computational efforts are required for the global minimum searches of these two relatively large clusters. The similarity between the PE spectrum of B_{41}^- and the main PES features of the planar B_{40}^- is helpful in the initial effort to search for the global minimum of B_{41}^-. We have found three low-lying 2D isomers (**I–III**) for B_{41}^-, which

are indeed related to the 2D structure of B_{40}^- and all are found to contribute to the observed PE spectrum, although isomer **II** (C_s, $^1A'$) of B_{41}^- with a DHV is found to be the main contributor. Many more low-lying isomers are found for B_{42}^-, including five 2D structures (**VII–XI**) and a tubular 3D isomer (**XII**, C_{2h}, ^2A_u). Two 2D isomers, **VIII** (C_1, ^2A) and **IX** (C_1, ^2A) of B_{42}^- both possessing a DHV, are found to be the major contributors to the experimental PE spectrum. The current work suggests that the 2D structural patterns, characteristic of the synthesized borophenes, continue in larger boron clusters beyond B_{40}^-, while borospherene cage isomers of B_{41}^- and B_{42}^- are much higher in energy.

2. Experimental and theoretical methods

2.1 Photoelectron spectroscopy

The experiments were carried out using a magnetic-bottle PES apparatus equipped with a laser vaporization cluster source, details of which can be found elsewhere.[6,80] Briefly, boron clusters were generated by laser vaporization of a hot-pressed ^{11}B-enriched disk target. The nascent clusters formed inside the nozzle were entrained by the He carrier gas seeded with 5% Ar and underwent a supersonic expansion to produce a cold cluster beam. Negatively charged clusters were extracted perpendicularly from the collimated cluster beam and analyzed using a time-of-flight mass spectrometer. The B_{41}^- and B_{42}^- clusters of current interest were mass-selected and decelerated before being photodetached by the 193 nm (6.424 eV) radiation from an ArF excimer laser. Photoelectrons were collected at nearly 100% efficiency and analyzed in a 3.5 m long electron flight tube. The photoelectron spectra were calibrated using the known spectrum of Bi^-. The resolution of the magnetic-bottle PES analyzer was $\Delta E_k/E_k \approx 2.5\%$, that is, ~25 meV for 1 eV kinetic energy electrons.

2.2 Computational methods

The global minima of B_{41}^- and B_{42}^- were searched using both the Tsinghua Global Minimum (TGMin) program[81–83] and the minima-hopping algorithm,[84,85] with the aid of extensive manual structural constructions based on the known low-lying isomers of B_{40}^-, B_{41}^+, and B_{42}^{2+}.[29,59] The TGMin code was interfaced to the CP2K program[86] and employed the DFT formalism with the PBE exchange–correlation functional[87] and the Goedecker–Teter–Hutter pseudopotential[88] with the associated double-ζ valence plus polarization basis set.[89] The global minimum search of B_{41}^- was assisted by the fact that its PE spectrum exhibited some similarity to that of the planar isomer of B_{40}^-, suggesting their structures should be related. In total, about 5000 structures were examined for B_{41}^- using TGMin, whereas 9745 structures were evaluated for B_{42}^-. In addition, more than 10 000 stationary points were probed using the minima-hopping method for B_{42}^-, locating similar low-lying isomers as the TGMin search. Low-lying isomers of B_{41}^- and B_{42}^- were reoptimized at the PBE0/6-311+G*

level,[90,91] which was proven to be a reliable method for boron clusters in this size range. All local minima were verified by calculations of the harmonic vibrational frequencies and the energies of all stable isomers were corrected by zero-point energies. For competitive low-lying isomers of B_{41}^- and B_{42}^-, we further did *ab initio* DLPNO-CCSD(T) and DLPNO-CCSD (DLPNO stands for domain-based local pair natural orbital) calculations[92,93] with the PBE0/6-311+G* geometries to obtain more accurate relative energies, respectively. The CCSD T_1 diagnostic factors were calculated to be small, within T_1 = 0.014–0.018 for the three lowest-lying isomers of B_{41}^- and 0.014–0.023 for the six lowest-lying isomers of B_{42}^-, indicating that the multi-configurational character was not significant. The vertical detachment energies (VDEs) of the lowest-lying isomers were calculated using the time-dependent DFT method (TDDFT-PBE0/6-311+G*) at the anion geometries.[94] The adiabatic detachment energies (ADEs) were computed as the energy differences of the anions and the corresponding neutrals at their respective optimized geometries at the PBE0/6-311+G* level of theory.

The electronic structure calculations at the PBE0 and TDDFT-PBE0 levels were done using the Gaussian 09 package,[95] whereas the DLPNO-CCSD(T) and DLPNO-CCSD calculations were performed with the ORCA suite of programs.[96] Chemical bonding analyses were done using the Adaptive Natural Density Partitioning (AdNDP) method[97] and were visualized using the VMD 1.9.3 software.[98]

3. Experimental results

The PE spectra of B_{41}^- and B_{42}^- at 193 nm are displayed in Fig. 1a and 2a, respectively, in comparison with the simulated spectra of the low-lying isomers. The spectra of the two clusters are fairly broad and the observed spectral features are labeled with letters (X, A, B, *etc.*). The experimental VDEs are summarized in Tables S1 and S2† and compared with the theoretical values given in the ESI.† The computed VDEs are plotted in Fig. 1 and 2 as vertical bars, which are fitted each with a unit area Gaussian to yield the simulated spectra.

3.1 The photoelectron spectrum of B_{41}^-

The experimental spectrum of B_{41}^- in Fig. 1a exhibits six broad bands (X, A, B, C, D, E). The first detachment channel of B_{41}^- is defined by band X with a VDE of 3.89 eV. The first ADE is estimated from its onset to be 3.71 eV, which also represents the electron affinity (EA) of the corresponding neutral B_{41}. There is a long tail on the low binding energy side of band X due to either vibrational hot bands or contributions from minor isomers. Following an energy gap of 0.51 eV, the well-separated band A is observed with a VDE of 4.40 eV. Beyond band A, the spectral features are nearly continuous, although band D at 5.80 eV is well defined. The broad features between bands A and D are labeled as B (~5.1 eV) and C (~5.4 eV) for the sake of discussion. There are likely multiple overlapping detachment channels in this spectral region. The spectrum is
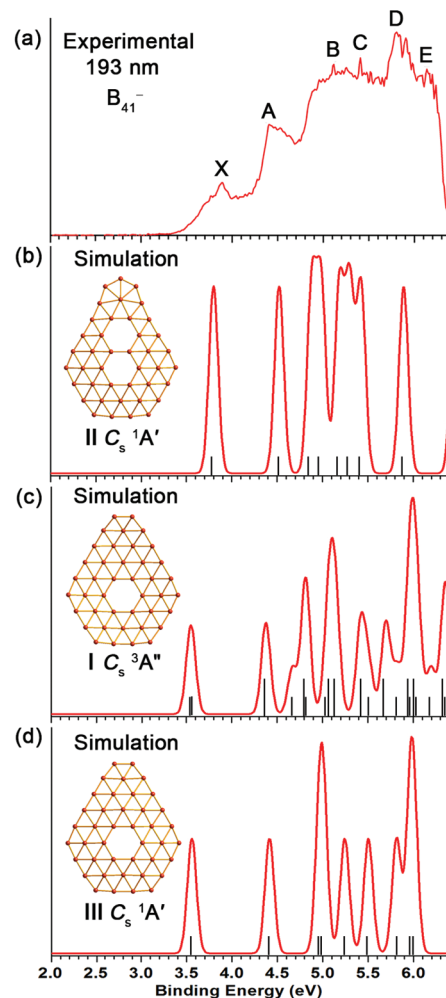

Fig. 1 Photoelectron spectrum of B_{41}^- at 193 nm (6.424 eV) (a), compared with simulated spectra of isomers **II** (b), **I** (c), and **III** (d). The theoretical VDEs were calculated at the TDDFT-PBE0/6-311+G* level and plotted as vertical bars. The simulated spectra were obtained by fitting the calculated VDEs with unit-area Gaussian functions of 0.1 eV half-width. In (c), the longer bars are for quartet final states and the shorter bars for doublet final states. See Table S1.†

cut off beyond 6.3 eV and a band *E* at ~6.1 eV is tentatively labeled.

The overall spectral pattern of B_{41}^- is quite similar to the main spectral features of B_{40}^- that was mainly due to the planar global minimum of B_{40}^-. The borospherene B_{40}^- was a slightly higher energy isomer in the anion and was present as a minor species with a very low electron binding energy.[29] The band X of B_{41}^- is similar to the band X of B_{40}^- at a VDE of 3.63 eV, except that the former is broader due to the low-binding energy tail. The higher electron binding energy of B_{41}^- is understandable because it is expected to be closed shell, whereas B_{40}^- with an odd number of electrons is open-shell. The band A of B_{41}^- is similar to the band A of B_{40}^- with a VDE of 4.24 eV. The higher binding energy features of B_{41}^- also display similarities to those in the B_{40}^- spectrum except that the features in B_{41}^- are more complicated mainly in the con-
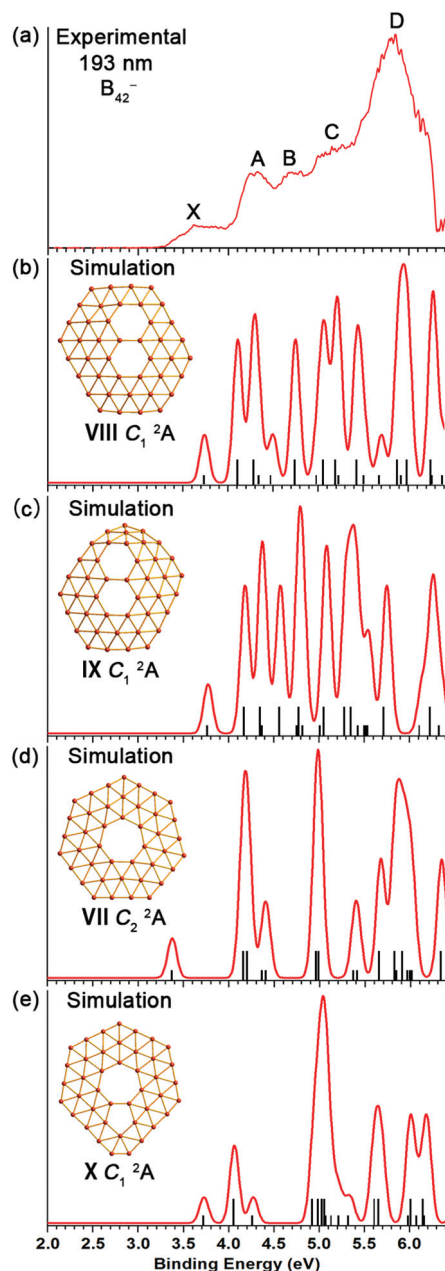
Fig. 2 Photoelectron spectrum of B_{42}^- at 193 nm (6.424 eV) (a), compared with simulated spectra of isomers **VIII** (b), **IX** (c), **VII** (d), and **X** (e). The theoretical VDEs were calculated at the TDDFT-PBE0/6-311+G* level and plotted as vertical bars. The simulated spectra were obtained by fitting the calculated VDEs with unit-area Gaussian functions of 0.1 eV half-width. The longer bars are for triplet final states and the shorter bars for singlet final states. See Table S2.†

gested B/C spectral region. The remarkable spectral similarity between B_{41}^- and B_{40}^- suggests that they may have similar structures, which is hugely helpful in the global minimum search for B_{41}^-.

3.2 The photoelectron spectrum of B_{42}^-

The PE spectrum of B_{42}^- is more diffuse and congested; five main spectral features are labeled (X, A, B, C, and D), as shown

Fig. 2a. The first band X is quite broad, ranging from ~3.3 to >4.0 eV, and centered around 3.61 eV. The broad band X is most likely due to contributions of multiple low-lying isomers or large geometry changes between the anionic and neutral ground states. The broad width of band X makes it difficult to evaluate the ADE, which is tentatively estimated to be 3.4 eV. Band A with a VDE of 4.31 eV is better defined and it is somewhat similar to the band A of B_{41}^- (VDE: 4.40 eV) (Fig. 1a). Bands B (4.66 eV) and C (~5.2 eV) are broad and overlap with each other. At the high binding energy side, one intense and broad feature D is observed at 5.84 eV. There must be multiple detachment transitions under each of the broad spectral bands. The B_{42}^- cluster is open-shell, and more complicated detachment features are partly expected, in addition to the possibility of multiple isomers.

4. Theoretical results

The global minima and low-lying isomers of B_{41}^- (**I–III**) and B_{42}^- (**VII–XII**) are depicted in Fig. 3 and 4, respectively. Alternative optimized low-lying isomers within about 2.80 eV of the global minima are given in Fig. S1† for B_{41}^- and Fig. S2† for B_{42}^-. Cartesian coordinates for the B_{41}^- (**I–III**) and B_{42}^- (**VII–XII**) isomers are listed in Table S3.†

4.1 The global minimum and low-lying isomers of B_{41}^-

Assisted by the observation that the PE spectrum of B_{41}^- is similar to that of the 2D isomer of B_{40}^-, we constructed the initial structures of B_{41}^- by adding one B atom to different sites of the 2D global minimum of B_{40}^- with a DHV.[29] The manually constructed structures and other alternative isomers obtained from the global minimum searches were fully reoptimized at the PBE0 level, and then the top three lowest-lying isomers were refined at the single-point CCSD(T) level, as shown in Fig. 3. Not surprisingly, these low-lying isomers are all related to the 2D global minimum of B_{40}^-. Isomer **I** with a triplet state (C_s, $^3A''$) is found to be the most stable structure of B_{41}^- at both the PBE0 and CCSD(T) levels of theory. It can be viewed as constructed by inserting one B atom into a hexagonal vacancy of the DHV in the global minimum 2D B_{40}^-.[29] The second lowest-lying isomer, **II** (C_s, $^1A'$), is 0.20 eV higher in energy at the CCSD(T) level. This isomer contains a DHV and can be constructed by inserting one B atom into the top edge of the 2D B_{40}^-. The third lowest-lying isomer of B_{41}^-, **III** (C_s, $^1A'$), which is 0.23 eV above the global minimum at the CCSD(T) level, is similar to the corresponding singlet state of the global minimum **I** (C_s, $^3A''$). The corresponding neutral structures are optimized at the PBE0 level and similar energetic ordering is found as the anions, as shown in Fig. 3 (**IV–VI**), except that the triplet isomer **I** of the anion is turned into a quartet state in the neutral (**VI**, C_s, $^4A''$).

The CCSD(T) results for the anions were deemed reliable on the basis of the small T_1 diagnostic factors, 0.018, 0.015, and 0.014 for isomers **I**, **II** and **III** of B_{41}^-, respectively. Considering the intrinsic accuracy of the theoretical methods, we should
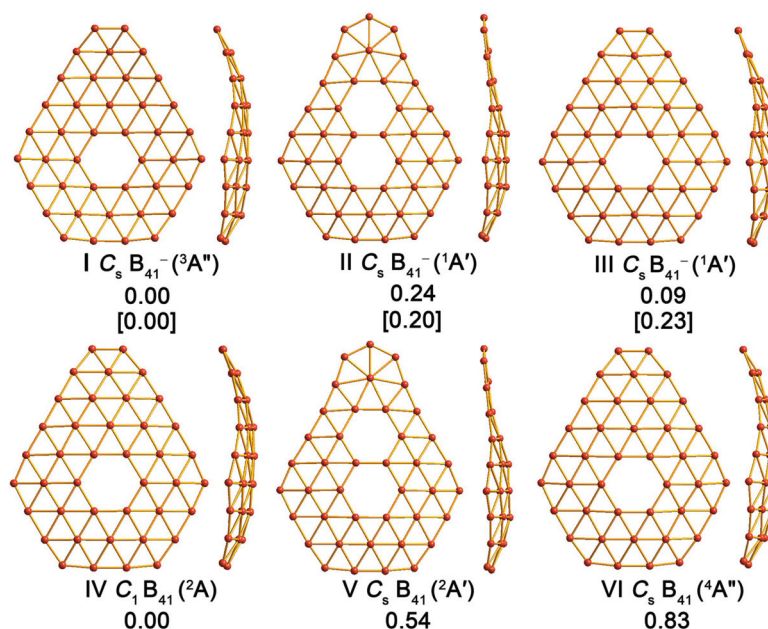
Fig. 3 The top three low-lying isomers of B_{41}^- (**I–III**) and their corresponding neutrals (**IV–VI**). Relative energies at the PBE0/6-311+G* level and single-point CCSD(T) level (in square brackets) at the PBE0/6-311+G* geometries are given in eV. The PBE0 energies are corrected for zero-point energies.

Fig. 4 The top six low-lying isomers of B_{42}^- (**VII–XII**) and their corresponding neutrals (**XIII–XVIII**). Relative energies at the PBE0/6-311+G* level and single-point CCSD level (in square brackets) at the PBE0/6-311+G* geometries are given in eV. The PBE0 energies are corrected for zero-point energies.
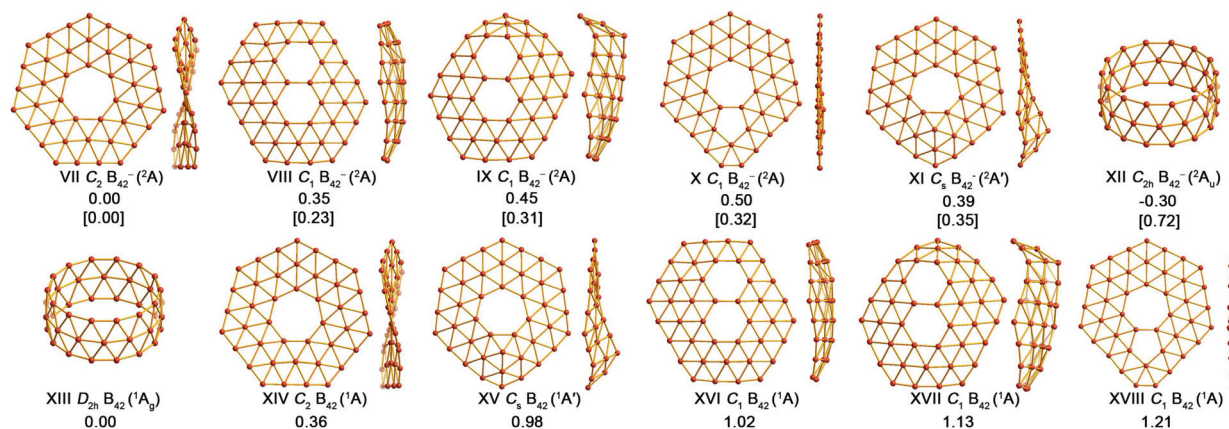
view that isomers **I–III** can all be candidates for the global minimum and they may coexist in the experiment. Alternative higher energy isomers of B_{41}^- presented in Fig. S1† are at least 0.34 eV higher in energy at the PBE0 level. It should be pointed out that two borospherene isomers, which are similar to the most stable and third lowest-lying isomers of B_{41}^+, respectively,[59] are found to be 1.15 and 1.32 eV higher in energy than the global minimum at the PBE0 level of theory (Fig. S1†).

4.2 The global minimum and low-lying isomers of B_{42}^-

Extensive global minimum searches, in conjunction with calculations at the PBE0/6-311-+G* level, revealed a very complex

potential energy landscape for B_{42}^- (Fig. S2†). Because of the large size and open-shell nature of B_{42}^-, only single-point CCSD/6-31G calculations based on the PBE0/6-311+G* structures could be afforded. The six low-lying isomers are shown in Fig. 4. At the PBE0 level, the global minimum is a tubular isomer (**XII**, C_{2h}, ^2A_u) with five 2D low-lying isomers consisting of a heptagonal vacancy or DHV. At the CCSD/6-31G level, the global minimum of B_{42}^- becomes isomer **VII** (C_2, ^2A) with a heptagonal vacancy, followed by two 2D isomers with a DHV (**VIII** and **IX**) and two 2D isomers with a heptagonal vacancy (**X** and **XI**). Isomer **X** also features a pentagonal vacancy. Isomers **VIII** (C_1, ^2A) and **IX** (C_1, ^2A) with a DHV can be derived from

the global minima of the B_{38}^- and B_{37}^- clusters[35] by adding four or five boron atoms to their longer edges. All these 2D isomers are within about 0.1 eV of each other and could all coexist in the experiment. We also optimized the corresponding neutral clusters at the PBE0 level of theory and their energetic ordering is similar to the anion at the same level of theory, as shown in Fig. 4 (**XIII–XVIII**).

Our global minimum searches also generated cage-like borosphere structures, which are all much higher in energy. The lowest borosphere isomer is 1.26 eV higher in energy than the global minimum at the PBE0 level of theory (Fig. S2†). Cartesian coordinates of the six lowest-lying structures of B_{42}^- (Fig. 4) are also given in Table S3.†

5. Comparison between experiment and theory

Because of the limited intrinsic accuracies of the theoretical methods, it is essential to compare theory and experiment to determine the true global minima of such large systems. To validate the computational results for B_{41}^- and B_{42}^-, we calculated the VDEs of their low-lying isomers for comparison with the experimental PE spectra.

5.1 B_{41}^-

The computed VDEs for the low-lying isomers **I–III** of B_{41}^- are given in Table S1† along with the experimental data. Each computed VDE is fitted with a Gaussian to produce the simulated spectra, which are compared with the experimental data in Fig. 1. The overall simulated spectral patterns of all three isomers agree well with the experimental spectrum, all with a large gap between the first and second bands. But the first VDE of isomer **II** agrees well with band X and the simulated spectrum of isomer **II** matches better with the experimental spectrum of B_{41}^-, relative to that of isomers **I** and **III**.

The calculated first VDE of isomer **II**, derived from the electron detachment from the HOMO (36a′), is 3.79 eV, in good agreement with the observed VDE of 3.89 eV for band X (Table S1†). The computed ADE of 3.73 eV for isomer **II** also agrees well with the measured ADE for band X (3.71 eV). The computed second VDE arising from the removal of an electron from the HOMO−1 (35a′) is 4.51 eV, which is consistent with the VDE of 4.40 eV observed for band A. The next five detachment channels are calculated to be within 4.87 eV and 5.42 eV, which agree well with the broad features designated as bands B and C. The next calculated detachment is at 5.89 eV, well separated from other detachment channel, in excellent agreement with the observed band D at 5.80 eV. Overall, the simulated spectrum of isomer **II** with a DHV can well reproduce the main spectral features in the PES experiment and isomer **II** should be the main species present in the cluster beam.

The calculated first VDEs for isomers **I** (3.53 eV) and **III** (3.55 eV) are slightly lower than the observed feature X (3.89 eV). These lower VDEs of isomers **I** and **III** likely correspond to the weak low binding energy tail of band X in the experimental

PE spectrum, providing experimental evidence for the presence of isomers **I** and **III** in the cluster beam of B_{41}^- as minor species. The combination of all three isomers explains well about the rather congested PE spectrum for B_{41}^-.

5.2 B_{42}^-

All the low-lying isomers of B_{42}^- have doublet spin states, and both singlet and triplet final states are possible upon one-electron detachment, resulting in more complicated detachment channels. The calculated VDEs for the top four isomers (**VII–X**) of B_{42}^- are given in Table S2† along with the experimental data and their simulated spectra are compared with the experimental PE spectrum in Fig. 2. The simulated spectra for two higher energy isomers **XI** and **XII** of B_{42}^- are compared with the experimental spectrum in Fig. S3.†

The simulated spectral patterns of isomers **VII** (Fig. 2d) and **X** (Fig. 2e) are relatively simple. They do not agree with the observed complicated spectral pattern and thus isomers **VII** and **X** can be immediately ruled out as the main contributors to the experimental spectrum, as well as isomers **XI** and **XII** (Fig. S3†). The simulated spectra of both isomers **VIII** and **IX** are fairly complicated; both are consistent with the congested experimental PE spectrum. The calculated first VDE for isomer **VIII** (VDE = 3.73 eV) is in good agreement with the experimental VDE of 3.61 eV for band X. The next four detachment channels, with calculated VDEs of 4.10, 4.28, 4.34 and 4.49 eV, are close to each other, agreeing well with the broad band A centered at 4.31 eV. The congested computed detachment channels at higher binding energies for isomer **VIII** (Fig. 2b) in general agree with the experimental spectrum, suggesting that isomer **VIII** with a DHV should be the main contributor to the observed PE spectrum. However, the broad X band in the experimental PE spectrum suggests that other isomers may be present. In particular, isomers **VII**, **IX**, and **X** could all be present as minor species in the cluster beam, giving rise to the broad X band and contributing to the congestion of the observed spectral features.

6. Structures and chemical bonding of B_{41}^- and B_{42}^-

6.1 The double-hexagonal vacancy in medium-sized 2D boron clusters

Comparisons between theory and experiment show that the 2D structures with a DHV are the major species observed in the PE spectra of B_{41}^- and B_{42}^-. Our previous investigations indicate that almost all of the global minima of negatively charged B_n^- (n = 3–40) clusters possess planar or quasi-planar global minima,[5–7,9–11] except the axially chiral B_{39}^- borosphere.[31] While the B_3 triangles are the characteristic structural units in boron chemistry, the 2D boron clusters exhibit various degrees of defects, from tetragonal, pentagonal, to hexagonal vacancies as the cluster size increases. Although the B_{36} cluster was the first boron cluster found to contain a hexagonal vacancy,[26] the hexagonal vacancy started to appear among the low-lying

isomers in the much smaller B_{26}^{-}.[37] The boron clusters with hexagonal vacancies can be viewed as building blocks to form boron monolayers with hexagonal vacancies and provide experimental evidence for the predicted 2D borons. The B_{35}^{-} cluster was the first boron cluster found to feature a DHV,[30] immediately following the discovery of the hexagonal B_{36}. The DHV seems to become a prevalent structural feature in larger 2D boron clusters, such as B_{37}^{-}, B_{38}^{-}, and the 2D global minimum of the B_{40}^{-} anion (C_s).[29,35] Hence, it is understandable that the true global minima of B_{41}^{-} and B_{42}^{-} both feature a DHV, in particular, the isomer **II** (C_s, $^1A'$) of B_{41}^{-} is directly related to the 2D global minimum of B_{40}^{-}, as revealed by the similarity of their PE spectra. The isomer **II** of B_{41}^{-} can be viewed as inserting one B atom to the edge of the 2D B_{40}^{-}, resulting in a spoon-like 2D structure (length: 12.1 Å, width: 9.6 Å) with an out-of-plane distortion of 1.42 Å. The out-of-plane distortion is mainly caused by the fact that the peripheral B–B σ bonds are stronger with shorter bond lengths, thus creating strains in the interior of the 2D systems, as clearly demonstrated by the transformation of the bowl-shaped aromatic B_{12} cluster to a perfectly planar AlB_{11} cluster because of the longer peripheral Al–B bonds.[99] The isomer **VIII** (C_1, ^2A) of B_{42}^{-} is directly associated with the C_s B_{38}^{-} and C_1 B_{37}^{-} clusters,[35] both containing a DHV with a bowl shape. The length, width and out-of-plane distortion of isomer **VIII** (C_1, ^2A) of B_{42}^{-} are 11.1 Å, 8.50 Å, and 1.68 Å, respectively. The DHV in the medium-sized 2D boron clusters is consistent with the observed χ^3 borophenes,[54,57,58] which feature rows of hexagonal vacancies. It would be interesting to see if such structural features will continue in larger boron clusters. An isomer with a row of three hexagonal vacancy is found in the global minimum search of B_{41}^{-}, but it is 2.77 eV higher than the global minimum at the PBE0 level (Fig. S1†).

6.2 Chemical bonding in the 2D isomers II (C_s, $^1A'$) of B_{41}^{-} and VIII (C_1, ^2A) of B_{42}^{-}: π aromaticity and analogy to the PAH $C_{27}H_{13}^{+}$

We analyzed the chemical bonding in isomer **II** (C_s, $^1A'$) of B_{41}^{-} using both AdNDP (Fig. 5)[97] and canonical MOs (Fig. S4†). The bonding pattern in B_{41}^{-} is similar to that in the C_s B_{40}^{-} due to their structural similarity.[29] As shown in Fig. 5a, the peripheral B_{21} ring and the inner B_2 bridge between the two hexagonal holes are described by twenty-two 2c–2e σ bonds. The bonding between the DHV and the surrounding boron atoms is *via* ten 3c–2e σ bonds, whereas the bonding between the peripheral B_{21} ring and the middle B_{14} ring is through twelve 3c–2e σ and five 4c–2e σ bonds. Also similar to those in the 2D B_{40}^{-}, there exist three types of π bonds in the C_s B_{41}^{-}. We found seven multi-centered (five 4c–2e and two 5c–2e) π bonds around the external apex sites mainly involving bonding between the peripheral B_{21} ring and the middle B_{14} ring. The bottom B_6 ring involves in three 11c–2e π bonds, which are similar to those in benzene. The third type of π bonds consist of the three completely delocalized 41c–2e π bonds. The π bonding pattern in B_{41}^{-} is also similar to the PAH $C_{27}H_{13}^{+}$, as shown Fig. 5b, continuing the all-boron
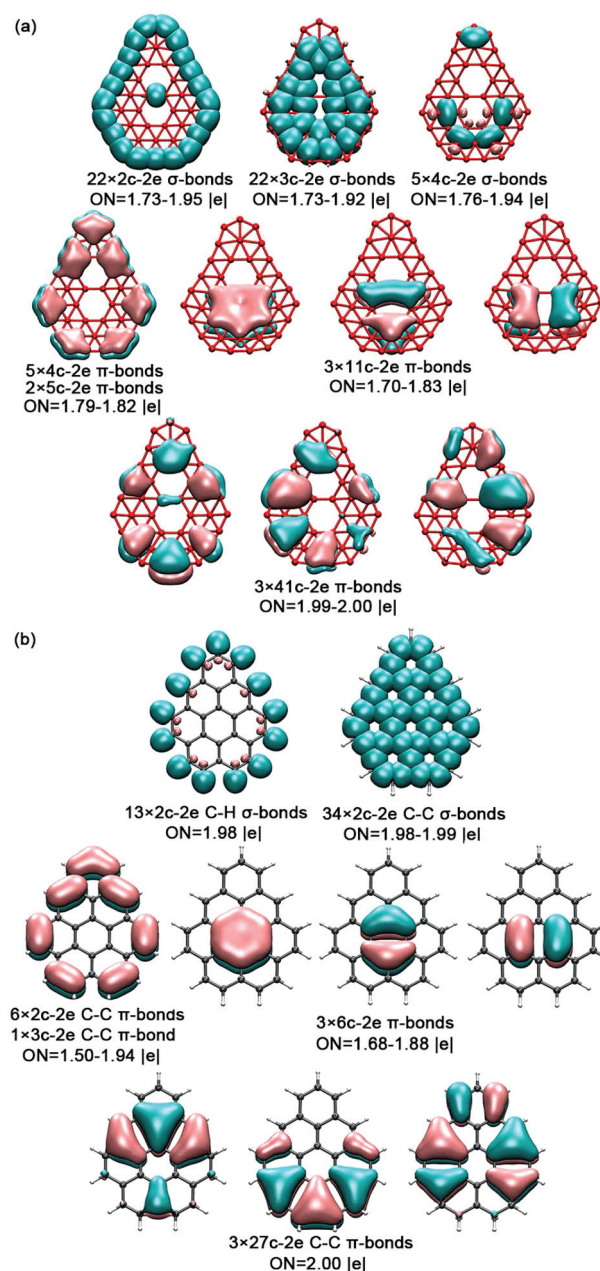

(a)

22×2c-2e σ-bonds
ON=1.73-1.95 |e|

22×3c-2e σ-bonds
ON=1.73-1.92 |e|

5×4c-2e σ-bonds
ON=1.76-1.94 |e|

5×4c-2e π-bonds
2×5c-2e π-bonds
ON=1.79-1.82 |e|

3×11c-2e π-bonds
ON=1.70-1.83 |e|

3×41c-2e π-bonds
ON=1.99-2.00 |e|

(b)

13×2c-2e C–H σ-bonds
ON=1.98 |e|

34×2c-2e C–C σ-bonds
ON=1.98-1.99 |e|

6×2c-2e C–C π-bonds
1×3c-2e C–C π-bond
ON=1.50-1.94 |e|

3×6c-2e π-bonds
ON=1.68-1.88 |e|

3×27c-2e C–C π-bonds
ON=2.00 |e|

Fig. 5 The AdNDP bonding analysis for (a) C_s B_{41}^{-} in comparison with that of (b) C_{2v} $C_{27}H_{13}^{+}$. Occupation numbers (ONs) are shown.

analogs of hydrocarbons by 2D boron clusters.[5–7,15,16,19–21] Comparison between the π MOs of the isomer **II** of B_{41}^{-} with those of $C_{27}H_{13}^{+}$ is given in Fig. S4,† where the MOs of the triplet isomer **I** of B_{41}^{-} are also shown. The AdNDP analysis of isomer **I** is given in Fig. S5.† The π bonding in isomer **I** is similar to that in isomer **II**, except that the two unpaired electrons in isomer **I** form two additional 41c–1e π bonds.

Instead of the open-shell isomer **VIII** (C_1, ^2A) of B_{42}^{-}, we analyzed the chemical bonding of the corresponding closed-shell neutral isomer **XVI** (C_1, ^1A) of B_{42} (Fig. 4), as shown in Fig. 6. The bonding in B_{42} is similar to that in B_{41}^{-}, in particular the π
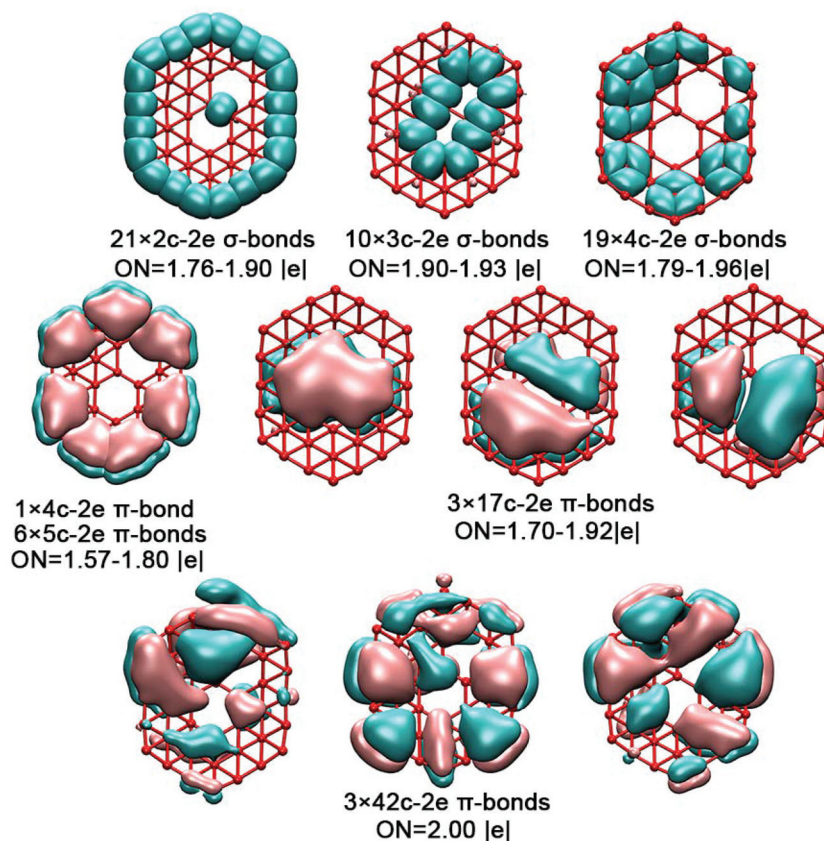
Fig. 6 The AdNDP bonding analysis for the planar closed-shell B_{42} isomer with a DHV (C_1, ^1A) corresponding to isomer **VIII** (C_1, ^2A) of the B_{42}^- anion (see Fig. 2). Occupation numbers (ONs) are shown.

bonding in the two systems are nearly identical. Thus, the 2D B_{42} with a DHV can also be considered as an all-boron analog of $C_{27}H_{13}^+$. The π MOs of B_{42} are compared with those of $C_{27}H_{13}^+$ in Fig. S6.† Therefore, the energetic advantages and stabilities of the 2D B_{41}^- and B_{42}^- structures with a DHV can be understood on the basis of their π aromaticity in analogy to the PAH $C_{27}H_{13}^+$. These results underscore the previously found structural and electronic analogy between boron clusters and hydrocarbons.[16]

7. Conclusions

We report a joint experimental and theoretical study of the B_{41}^- and B_{42}^- clusters, the largest boron clusters characterized experimentally to date. The photoelectron spectra of the two clusters were obtained and were shown to be quite broad and complicated. Three low-lying isomers were found for B_{41}^-, one quasi-planar isomer **II** (C_s, $^1A'$) with a DHV and two quasi-planar isomers **I** (C_s, $^3A''$) and **III** (C_s, $^1A'$) with one hexagonal vacancy. The simulated spectrum for isomer **II** was found to be the major contributor to the experimental spectrum, with isomers **I** and **III** as possible minor species present in the experiment. Isomer **II** of B_{41}^- can be viewed as inserting a B atom to the edge of the 2D B_{40}^- structure, consistent with the similarity of their PE spectra. A much more complicated potential energy landscape

was found for B_{42}^-, for which six low-lying isomers were uncovered. Isomer **VIII** (C_1, ^2A) with a DHV was found to be the dominating contributor to the observed spectrum, while isomer **IX** (C_1, ^2A) also with a DHV gives a similarly complicated simulated spectrum and cannot be ruled out. The very broad first PES band suggests that other low-lying isomers **VII**, **X**, and **XI** could also exist as minor species in the experiment. Chemical bonding analyses reveal that the isomer **II** (C_s, $^1A'$) of B_{41}^- and isomer **VIII** (C_1, ^2A) of B_{42}^- are aromatic, analogous to the PAH $C_{27}H_{13}^+$ in their π-bonding, extending the concept of all-boron analogs of polycyclic aromatic hydrocarbons to B_{41}^- and B_{42}. The current study shows that boron clusters beyond B_{40} still prefer 2D structures with multiple hexagonal vacancies, underlying the structural stability of borophenes. Borospherene cage isomers for both clusters are found to be much higher in energy.

Conflicts of interest

There are no conflicts to declare.

Acknowledgements

Notes and references

1 B. Albert and H. Hillebrecht, *Angew. Chem., Int. Ed.*, 2009, **48**, 8640.

2 A. R. Oganov, J. Chen, C. Gatti, Y. Ma, Y. Ma, C. W. Glass, Z. Liu, T. Yu, O. O. Kurakevych and V. L. Solozhenko, *Nature*, 2009, **457**, 863.

3 A. N. Alexandrova, A. I. Boldyrev, H. J. Zhai and L. S. Wang, *Coord. Chem. Rev.*, 2006, **250**, 2811.

4 E. Oger, N. R. M. Crawford, R. Kelting, P. Weis, M. M. Kappes and R. Ahlrichs, *Angew. Chem., Int. Ed.*, 2007, **46**, 8503.

5 A. P. Sergeeva, I. A. Popov, Z. A. Piazza, W. L. Li, C. Romanescu, L. S. Wang and A. I. Boldyrev, *Acc. Chem. Res.*, 2014, **47**, 1349.

6 L. S. Wang, *Int. Rev. Phys. Chem.*, 2016, **35**, 69.

7 A. I. Boldyrev and L. S. Wang, *Phys. Chem. Chem. Phys.*, 2016, **18**, 11589.

8 M. R. Fagiani, X. W. Song, P. Petrov, S. Debnath, S. Gewinner, W. Schollkopf, T. Heine, A. Fielicke and K. R. Asmis, *Angew. Chem., Int. Ed.*, 2017, **56**, 501.

9 W. L. Li, H. S. Hu, Y. F. Zhao, X. Chen, T. T. Chen, T. Jian, L. S. Wang and J. Li, *Sci. Sin.: Chim.*, 2018, **48**, 98.

10 W. L. Li, X. Chen, T. Jian, T. T. Chen, J. Li and L. S. Wang, *Nat. Rev. Chem.*, 2017, **1**, 0071.

11 T. Jian, X. N. Chen, S. D. Li, A. I. Boldyrev, J. Li and L. S. Wang, *Chem. Soc. Rev.*, 2019, **48**, 3550.

12 H. J. Zhai, L. S. Wang, A. N. Alexandrova and A. I. Boldyrev, *J. Chem. Phys.*, 2002, **117**, 7917.

13 A. N. Alexandrova, A. I. Boldyrev, H. J. Zhai, L. S. Wang, E. Steiner and P. W. Fowler, *J. Phys. Chem. A*, 2003, **107**, 1359.

14 H. J. Zhai, L. S. Wang, A. N. Alexandrova, A. I. Boldyrev and V. G. Zakrzewski, *J. Phys. Chem. A*, 2003, **107**, 9319.

15 H. J. Zhai, A. N. Alexandrova, K. A. Birch, A. I. Boldyrev and L. S. Wang, *Angew. Chem., Int. Ed.*, 2003, **42**, 6004.

16 H. J. Zhai, B. Kiran, J. Li and L. S. Wang, *Nat. Mater.*, 2003, **2**, 827.

17 A. N. Alexandrova, A. I. Boldyrev, H. J. Zhai and L. S. Wang, *J. Phys. Chem. A*, 2004, **108**, 3509.

18 B. Kiran, S. Bulusu, H. J. Zhai, S. Yoo, X. C. Zeng and L. S. Wang, *Proc. Natl. Acad. Sci. U. S. A.*, 2005, **102**, 961.

19 A. P. Sergeeva, D. Y. Zubarev, H. J. Zhai, A. I. Boldyrev and L. S. Wang, *J. Am. Chem. Soc.*, 2008, **130**, 7244.

20 W. Huang, A. P. Sergeeva, H. J. Zhai, B. B. Averkiev, L. S. Wang and A. I. Boldyrev, *Nat. Chem.*, 2010, **2**, 202.

21 A. P. Sergeeva, B. B. Averkiev, H. J. Zhai, A. I. Boldyrev and L. S. Wang, *J. Chem. Phys.*, 2011, **134**, 224304.

22 Z. A. Piazza, W. L. Li, C. Romanescu, A. P. Sergeeva, L. S. Wang and A. I. Boldyrev, *J. Chem. Phys.*, 2012, **136**, 104310.

23 A. P. Sergeeva, Z. A. Piazza, C. Romanescu, W. L. Li, A. I. Boldyrev and L. S. Wang, *J. Am. Chem. Soc.*, 2012, **134**, 18065.

24 C. Romanescu, D. J. Harding, A. Fielicke and L. S. Wang, *J. Chem. Phys.*, 2012, **137**, 014317.

25 I. A. Popov, Z. A. Piazza, W. L. Li, L. S. Wang and A. I. Boldyrev, *J. Chem. Phys.*, 2013, **139**, 144307.

26 Z. A. Piazza, H. S. Hu, W. L. Li, Y. F. Zhao, J. Li and L. S. Wang, *Nat. Commun.*, 2014, **5**, 3113.

27 W. L. Li, Y. F. Zhao, H. S. Hu, J. Li and L. S. Wang, *Angew. Chem., Int. Ed.*, 2014, **53**, 5540.

28 Z. A. Piazza, I. A. Popov, W. L. Li, R. Pal, X. C. Zeng, A. I. Boldyrev and L. S. Wang, *J. Chem. Phys.*, 2014, **141**, 034303.

29 H. J. Zhai, Y. F. Zhao, W. L. Li, Q. Chen, H. Bai, H. S. Hu, Z. A. Piazza, W. J. Tian, H. G. Lu, Y. B. Wu, Y. W. Mu, G. F. Wei, Z. P. Liu, J. Li, S. D. Li and L. S. Wang, *Nat. Chem.*, 2014, **6**, 727.

30 W. L. Li, Q. Chen, W. J. Tian, H. Bai, Y. F. Zhao, H. S. Hu, J. Li, H. J. Zhai, S. D. Li and L. S. Wang, *J. Am. Chem. Soc.*, 2014, **136**, 12257.

31 Q. Chen, W. L. Li, Y. F. Zhao, S. Y. Zhang, H. S. Hu, H. Bai, H. R. Li, W. J. Tian, H. G. Lu, H. J. Zhai, S. D. Li, J. Li and L. S. Wang, *ACS Nano*, 2015, **9**, 754.

32 W. L. Li, R. Pal, Z. A. Piazza, X. C. Zeng and L. S. Wang, *J. Chem. Phys.*, 2015, **142**, 204305.

33 Y. J. Wang, Y. F. Zhao, W. L. Li, T. Jian, Q. Chen, X. R. You, T. Ou, X. Y. Zhao, H. J. Zhai, S. D. Li, J. Li and L. S. Wang, *J. Chem. Phys.*, 2016, **144**, 064307.

34 H. R. Li, T. Jian, W. L. Li, C. Q. Miao, Y. J. Wang, Q. Chen, X. M. Luo, K. Wang, H. J. Zhai, S. D. Li and L. S. Wang, *Phys. Chem. Chem. Phys.*, 2016, **18**, 29147.

35 Q. Chen, W. J. Tian, L. Y. Feng, H. G. Lu, Y. W. Mu, H. J. Zhai, S. D. Li and L. S. Wang, *Nanoscale*, 2017, **9**, 4550.

36 J. Czekner, L. F. Cheung and L. S. Wang, *J. Phys. Chem. C*, 2017, **121**, 10752.

37 X. M. Luo, T. Jian, L. J. Cheng, W. L. Li, Q. Chen, R. Li, H. J. Zhai, S. D. Li, A. I. Boldyrev, J. Li and L. S. Wang, *Chem. Phys. Lett.*, 2017, **683**, 336.

38 Q. Chen, W. L. Li, X. Y. Zhao, H. R. Li, L. Y. Feng, H. J. Zhai, S. D. Li and L. S. Wang, *Eur. J. Inorg. Chem.*, 2017, **2017**, 4546.

39 Q. Chen, T. T. Chen, H. R. Li, X. Y. Zhao, W. J. Chen, H. J. Zhai, S. D. Li and L. S. Wang, *Nanoscale*, 2019, **11**, 9698.

40 W. N. Lipscomb, *Science*, 1977, **196**, 1047.

41 J. Zhao, X. Huang, R. Shi, H. Liu, Y. Su and R. B. King, *Nanoscale*, 2015, **7**, 15086.

42 J. O. C. Jimenez-Halla, R. Islas, T. Heine and G. Merino, *Angew. Chem., Int. Ed.*, 2010, **49**, 5668.

43 G. Martinez-Guajardo, A. P. Sergeeva, A. I. Boldyrev, T. Heine, J. M. Ugalde and G. Meino, *Chem. Commun.*, 2011, **47**, 6242.

44 J. Zhang, A. P. Sergeeva, M. Sparta and A. N. Alexandrova, *Angew. Chem., Int. Ed.*, 2012, **51**, 8512.

45 D. Moreno, S. Pan, L. L. Zeonjuk, R. Islas, E. Osorio, G. Martinez-Guajardo, P. Chattaraj, T. Heine and G. Merino, *Chem. Commun.*, 2014, **50**, 8140.

46 H. Tang and S. Ismail-Beigi, *Phys. Rev. Lett.*, 2007, **99**, 115501.

47 X. Yang, Y. Ding and J. Ni, *Phys. Rev. B: Condens. Matter Mater. Phys.*, 2008, **77**, 041402.

48 K. C. Lau and R. Pandey, *J. Phys. Chem. B*, 2008, **112**, 10217.

49 E. S. Penev, S. Bhowmick, A. Sadrzadeh and B. I. Yakobson, *Nano Lett.*, 2012, **12**, 2441.

50 X. J. Wu, J. Dai, Y. Zhao, Z. W. Zhuo, J. L. Yang and X. C. Zeng, *ACS Nano*, 2012, **6**, 7443.

51 X. Yu, L. Li, X. X. Xu and C. C. Tang, *J. Phys. Chem. C*, 2012, **116**, 20075.

52 H. Lu, Y. Mu, H. Bai, Q. Chen and S. D. Li, *J. Chem. Phys.*, 2013, **138**, 024701.

53 A. J. Mannix, X. F. Zhou, B. Kiraly, J. D. Wood, D. Alducin, B. D. Myers, X. Liu, B. L. Fisher, U. Santiago, J. R. Guest, M. J. Yacaman, A. Ponce, A. R. Oganov, M. C. Hersam and N. P. Guisinger, *Science*, 2015, **350**, 1513.

54 B. Feng, J. Zhang, Q. Zhong, W. Li, S. Li, H. Li, P. Cheng, S. Meng, L. Chen and K. Wu, *Nat. Chem.*, 2016, **8**, 563.

55 Y. Liu, E. S. Penev and B. I. Yakobson, *Angew. Chem., Int. Ed.*, 2013, **52**, 3156.

56 H. Liu, J. Gao and J. Zhao, *Sci. Rep.*, 2013, **3**, 3238.

57 S. Xu, Y. Zhao, J. Liao, X. Yang and H. Xu, *Nano Res.*, 2016, **9**, 2616.

58 Z. Zhang, A. J. Mannix, Z. Hu, B. Kiraly, N. P. Guisinger, M. C. Hersam and B. I. Yakobson, *Nano Lett.*, 2016, **16**, 6622.

59 Q. Chen, S. Y. Zhang, H. Bai, W. J. Tian, T. Gao, H. R. Li, C. Q. Miao, W. Mu, H. G. Lu, H. J. Zhai and S. D. Li, *Angew. Chem., Int. Ed.*, 2015, **54**, 1.

60 T. B. Tai and M. T. Nguyen, *Chem. Commun.*, 2016, **52**, 1653.

61 L. W. Sai, X. Wu, N. Gao, J. J. Zhao and R. B. King, *Nanoscale*, 2017, **9**, 13905.

62 A. B. Rahane and V. Kumar, *Nanoscale*, 2015, **7**, 4055.

63 T. B. Tai, S. U. Lee and M. T. Nguyen, *Phys. Chem. Chem. Phys.*, 2016, **18**, 11520.

64 J. Kunstmann, V. Bezugly, H. Rabbel, M. H. Rummeli and G. Cuniberti, *Adv. Funct. Mater.*, 2014, **24**, 4127.

65 T. B. Tai and M. T. Nguyen, *RSC Adv.*, 2017, **7**, 22243.

66 X. L. Sheng, Q. B. Yan, Q. R. Zheng and G. Su, *Phys. Chem. Chem. Phys.*, 2009, **11**, 9696.

67 J. T. Muya, G. Gopakumar, M. T. Nguyen and A. Ceulemans, *Phys. Chem. Chem. Phys.*, 2011, **13**, 7524.

68 C. Ozdogan, S. Mukhopadhyay, W. Hayami, Z. B. Güvenc, R. Pandey and I. Boustani, *J. Phys. Chem. C*, 2010, **114**, 4362.

69 S. Polad and M. Ozay, *Phys. Chem. Chem. Phys.*, 2013, **15**, 19819.

70 H. T. Pham, J. T. Muya, F. Buendia, A. Ceulemans and M. T. Nguyen, *Phys. Chem. Chem. Phys.*, 2019, **21**, 7039.

71 N. G. Szwacki, A. Sadrzadeh and B. I. Yakobson, *Phys. Rev. Lett.*, 2007, **98**, 166804.

72 N. G. Szwacki, *Nanoscale Res. Lett.*, 2008, **3**, 49.

73 R. R. Zope, T. Baruah, K. C. Lau, A. Y. Liu, M. R. Pederson and B. I. Dunlap, *Phys. Rev. B: Condens. Matter Mater. Phys.*, 2009, **79**, 161403.

74 Q. B. Yan, X. L. Sheng, Q. R. Zheng, L. Z. Zhang and G. Su, *Phys. Rev. B: Condens. Matter Mater. Phys.*, 2008, **78**, 201401.

75 L. Wang, J. Zhao, F. Li and Z. Chen, *Chem. Phys. Lett.*, 2010, **501**, 16.

76 D. L. V. K. Prasad and E. D. Jemmis, *Phys. Rev. Lett.*, 2008, **100**, 165504.

77 S. De, A. Willand, M. Amsler, P. Pochet, L. Genovese and S. Goedecker, *Phys. Rev. Lett.*, 2011, **106**, 225502.

78 F. Y. Li, P. Jin, D. E. Jiang, L. Wang, S. B. Zhang, J. Zhao and Z. Chen, *J. Chem. Phys.*, 2012, **136**, 074302.

79 P. Boulanger, M. Moriniere, L. Genovese and P. Pochet, *J. Chem. Phys.*, 2013, **138**, 184302.

80 L. S. Wang, H. S. Cheng and J. Fan, *J. Chem. Phys.*, 1995, **102**, 9480.

81 Y. F. Zhao, X. Chen and J. Li, *Nano Res.*, 2017, **10**, 3407.

82 X. Chen, Y. F. Zhao, L. S. Wang and J. Li, *Comput. Theor. Chem.*, 2017, **1107**, 57.

83 X. Chen, Y. F. Zhao, Y. Y. Zhang and J. Li, *J. Comput. Chem.*, 2019, **40**, 1105.

84 S. Goedecker, *J. Chem. Phys.*, 2004, **120**, 9911.

85 S. Goedecker, W. Hellmann and T. Lenosky, *Phys. Rev. Lett.*, 2005, **95**, 055501.

86 J. VandeVondele, M. Krack, F. Mohamed, M. Parrinello, T. Chassaing and J. Hutter, *Comput. Phys. Commun.*, 2005, **167**, 103.

87 J. P. Perdew, K. Burke and M. Ernzerhof, *Phys. Rev. Lett.*, 1996, **77**, 3865.

88 S. Goedecker, M. Teter and J. Hutter, *Phys. Rev. B: Condens. Matter*, 1996, **54**, 1703.

89 J. VandeVondele and J. Hutter, *J. Chem. Phys.*, 2007, **127**, 114105.

90 C. Adamo and V. Barone, *J. Chem. Phys.*, 1999, **110**, 6158.

91 R. Krishnan, J. S. Binkley, R. Seeger and J. A. Pople, *J. Chem. Phys.*, 1980, **72**, 650.

92 C. Riplinger and F. Neese, *J. Chem. Phys.*, 2013, **138**, 034106.

93 C. Riplinger, B. Sandhoefer, A. Hansen and F. Neese, *J. Chem. Phys.*, 2013, **139**, 134101.

94 R. Bauernschmitt and R. Ahlrichs, *Chem. Phys. Lett.*, 1996, **256**, 454.

95 M. J. Frisch, *et al.*, *Gaussian 09, Revision D.01*, Gaussian, Inc., Wallingford, CT, 2009.

96 F. Neese, *Wiley Interdiscip. Rev.: Comput. Mol. Sci.*, 2012, **2**, 73.

97 D. Y. Zubarev and A. I. Boldyrev, *Phys. Chem. Chem. Phys.*, 2008, **10**, 5207.

98 W. Humphrey, A. Dalke and K. Schulten, *J. Mol. Graphics*, 1996, **14**, 33.

99 C. Romanescu, A. P. Sergeeva, W. L. Li, A. I. Boldyrev and L. S. Wang, *J. Am. Chem. Soc.*, 2011, **133**, 8646.